Published in final edited form as:
Neurobiol Aging. 2013 December ; 34(12): 2835–2842. doi:10.1016/j.neurobiolaging.2013.05.030.

Memory decline shows stronger associations with estimated spatial patterns of amyloid deposition progression than total amyloid burden

Rachel A. Yotter, PhD[1], **Jimit Doshi, MS**[1], **Vanessa Clark, PhD**[1], **Jitka Sojkova, MD**[2,3], **Yun Zhou, PhD**[3], **Dean F. Wong, MD, PhD**[3], **Luigi Ferrucci, MD, PhD**[4], **Susan M. Resnick, PhD**[2], and **Christos Davatzikos, PhD**[1]

[1]Section for Biomedical Image Analysis, Department of Radiology, University of Pennsylvania, Philadelphia, PA 19104, USA

[2]Laboratory of Behavioral Neuroscience, National Institute on Aging, Baltimore, MD 21224, USA

[3]Department of Radiology, Johns Hopkins School of Medicine, Baltimore, MD

[4]Longitudinal Studies Section, National Institute on Aging, Baltimore, MD

Abstract

The development of amyloid imaging compounds has allowed in vivo imaging of amyloid deposition. In this study, we examine the spatial patterns of amyloid deposition throughout the brain using Pittsburgh Compound Blue (11C-PiB) PET data from the Baltimore Longitudinal Study of Aging. We used a new methodology that allows us to approximate spatial patterns of the temporal progression of amyloid plaque deposition from cross-sectional data. Our results are consistent with patterns of progression known from autopsy studies, with frontal and precuneus regions affected early and occipital and sensorimotor cortices affected later in disease progression – here, disease progression means lower-to-higher total amyloid burden. Furthermore, we divided participants into subgroups based on longitudinal change in memory performance and demonstrated significantly different spatial patterns of the estimated progression of amyloid deposition between these subgroups. Our results indicate that the spatial pattern of amyloid deposition is related to cognitive performance and may be more informative than a biomarker reflecting total amyloid burden, which is the current practice. This finding has broad implications for our understanding of the relationship between cognitive decline/resilience and amyloid deposition, as well as for the use of amyloid imaging as a biomarker in research and clinical applications.

Keywords

Amyloid; PiB; PET; CVLT; cognition

Author Contact: Rachel A. Yotter, rachel.yotter@uphs.upenn.edu, Section for Biomedical Image Analysis, Department of Radiology, University of Pennsylvania, 3600 Market Street, Suite 380, Philadelphia, PA 19104, USA, +1-215-662-3110.

DISCLOSURE STATEMENT. The authors have nothing to disclose.

Introduction

The hallmark pathologies of Alzheimer's disease are histology-confirmed amyloid plaques and neurofibrillary tangles. Currently, disease progression must usually be estimated from cross-sectional data and is defined as lower-to-higher total pathology. As shown in a large series of post-mortem brains studied by Braak and Braak (Braak and Braak, 1997b), the progression of amyloid plaque deposition (both diffuse and neuritic) follows characteristic spatially unique stages rather than uniform deposition throughout the brain. There are substantial inter-individual variations in spatial patterns of amyloid deposition, but frontal, lateral temporal, and parietal regions are affected early, with relative sparing of the occipital lobe and motor cortices until later in disease progression.

Spatial heterogeneity of patterns of amyloid deposition have also been found using recently-developed in vivo amyloid tracers (Lockhart et al., 2007). Across studies, elevated amyloid deposition has been found in frontal cortex, lateral temporal cortex, and precuneus, especially in subjects with dementia of the Alzheimer type (DAT), with less consistent binding in the occipital cortex (Klunk et al., 2004; Lopresti et al., 2005; Rowe et al., 2008; Wong et al., 2010). A significant proportion of cognitively normal subjects also display elevated cortical amyloid burden (Jack et al., 2008; Pike et al., 2007), with some likely in the preclinical stages of DAT. In addition, patients with mild cognitive impairment (MCI) show a bimodal distribution, such that some subjects exhibit amyloid deposition similar to that of DAT subjects while other subjects exhibit deposition similar to healthy controls (Mintun et al., 2006; Villemagne et al., 2011; Villemagne et al., 2008). Furthermore, MCI subjects who exhibit amyloid burden similar to DAT subjects are more likely to progress to DAT, compared to subjects who exhibit levels of amyloid burden similar to healthy controls (Forsberg et al., 2008).

Mean or regional cortical amyloid burden are the typical biomarkers measured in *in vivo* amyloid imaging studies. Advances in *in vivo* imaging techniques methods now allow us to investigate temporal changes in amyloid deposition and relation to other imaging modalities in greater detail (Shoghi-Jadid et al., 2002; Sojkova et al., 2011b). Moreover, the spatiotemporal dynamics of amyloid deposition have not been studied in detail, in part due to the relatively recent availability of amyloid imaging radiotracers and the time lag in acquiring sufficient longitudinal data. In the current study, we use a pseudo-dynamic image analysis method, similar to that used by Braak and Braak, estimating the progression of amyloid deposition from cross-sectional images of older individuals. In particular, nonlinear regional fits are used to determine regional amyloid burden as a function of total amyloid load, thereby generating maps that indicate how much amyloid must be accumulated globally in the brain before a given brain region is affected. This is accomplished by making an assumption that total amyloid burden is related to temporal dynamics, i.e., a cortex will have lower total amyloid load earlier in the disease progression, and progressively higher amyloid load later in the disease progression, albeit a spline smoothing process is used to handle deviations from this assumption. Pseudo-temporal maps can then be generated from cross-sectional data. These maps are herein found to provide insights into the dynamics of amyloid spread throughout the brain that are not evident in conventional group comparisons.

While cross-sectional studies of relationships between amyloid burden and cognition have yielded mixed results, higher amyloid burden has been associated with greater longitudinal memory decline in a number of studies (for a review, see (Resnick and Sojkova, 2011)). In prior work, we have demonstrated associations between rates of longitudinal change in verbal episodic memory performance and structural/functional changes in the cortex (Clark et al., in press). Thus, in the present study, we aimed to use rates of change in California Verbal Learning Test (CVLT) scores to group participants for comparison of amyloid

progression patterns. Decline in verbal episodic memory is typically the earliest change during the prodromal phase of DAT (Grober et al., 2008).

Analyses of amyloid deposition patterns in relation to cognitive performance that have been based on region-of-interest or voxel-wise approaches have resulted in heterogeneous findings. Generally, the regions that appear to be more involved in episodic memory changes include the precuneus, also the frontal, posterior cingulate, and lateral parietal cortices (Rentz et al., 2011), and the (frontal and lateral) temporal regions (Chetelat et al., 2011; Resnick et al., 2010). Although these analyses begin to address differential associations between cognition and amyloid deposition across the cortex, they are confounded by high inter-individual variability introduced by the fact that different individuals enrolled in a study are generally at different stages of amyloid progression, which may obscure relationships between the spatial distribution and progression of amyloid and cognition. In other words, the same value of amyloid burden at a given spatial location might relate differently to cognitive decline, depending on the overall spatial pattern of deposition and the stage of the disease. Moreover, amyloid imaging, based on conventional measurements obtained from cross-sectional snapshots, is not very informative of the dynamics of disease progression. In order to mitigate this problem, we undertook to investigate spatial patterns of amyloid deposition as a function of total amyloid burden throughout the brain, such that total amyloid burden is used as a proxy for the underlying stage of disease progression in the absence of a more precise measure. Furthermore, we sought to determine whether the spatial patterns of amyloid deposition between subgroups would show a striking and significant divergence when individuals are classified according to longitudinal change in cognitive performance. A varying spatial pattern may indicate an earlier involvement of many specific brain regions in cognitive decliners (CD) compared with a relatively more constrained amyloid spread in cognitively stable (CS) individuals.

Methods

Participants

A series of 64 participants (35 men, 29 women; age [SD] 76.61 years [6.89]; cortical distributed volume ratio [SD] 1.16 [0.26]) from the Baltimore Longitudinal Study of Aging (BLSA) neuroimaging sub-study were included. Additional participants were evaluated but excluded due to clinical stroke (N=2), brain injury (N=1), and intolerance of MRI (N=1). At baseline, BLSA neuroimaging participants were excluded for the following conditions: CNS disease, severe cardiovascular disease, severe pulmonary disease, or metastatic cancer. The participants included in this study were representative of the entire BLSA group with respect to baseline age, sex, race, and education. For participants with multiple ^{11}C-PiB scans, only the last available scan was included for analysis.

All participants also underwent thorough neuropsychological evaluation in conjunction with each neuroimaging visit. Participants were followed for an average of 12 years (SD = 1.8 years) and were tested approximately once per year, resulting in an average of 11 test time-points per participant (SD = 1.57). A battery of 12 neuropsychological tests was administered at each neuroimaging visit to evaluate mental status, word knowledge and verbal ability, memory, language, verbal fluency, attention, executive function, and spatial ability. Mental status was assessed with the Mini-Mental State Examination (MMSE); verbal memory was assessed using the CVLT; and visual memory with the Benton Visual Retention Test (BVRT). Ten participants had a score of 0.5 or higher on the Clinical Dementia Rating (CDR) scale (Morris, 1997), of whom three were clinically diagnosed with MCI at the time of the scan, and one had a dementia diagnosis with subsequent autopsy-confirmed DAT. The CDR scale, typically informant-based, was administered in conjunction with ^{11}C-PiB PET imaging, and was also administered during earlier imaging

visits if participants scored 3 or more on the Blessed Information Memory Concentration test and at each visit for autopsy study participants (around 50% of the sample) (Blessed et al., 1968).

^{11}C-PiB PET Imaging

Dynamic ^{11}C-PiB PET studies (29 time frames over 70 minutes) were performed in 3D mode on a GE Advance scanner. Participants were fitted with a thermoplastic mask for PET imaging to minimize motion artifacts. The PET scanning started immediately after IV bolus injection of a mean (SD) 14.65 (0.9) mCi of ^{11}C-PiB. Dynamic images were reconstructed using filtered back-projection with a ramp filter (image size = 128 × 128, pixel size = 2 × 2 mm, slice thickness = 4.25 mm), yielding a spatial resolution of approximately 4.5 mm FWHM at the center of the field of view.

Quantification of ^{11}C-PiB distribution volume ratios (DVRs)

In conjunction with ^{11}C-PiB PET imaging, each participant also underwent structural MRI imaging with a T1-weighted volumetric protocol. MRI images were co-registered to the mean of the first 20-minute dynamic PET images for each participant using the mutual information method in the Statistical Parametric Mapping software (SPM2; Wellcome Department of Cognitive Neurology, London, UK). In addition to the cerebellum, which was used as a reference region, 15 regions of interest were manually drawn on the co-registered MRIs and used for region-of-interest (ROI) definition on the PET scans (Price et al., 2005).

The DVRs of ROIs were estimated by simultaneous fitting of a simplified reference tissue model using linear regression with spatial constraints (SRTM-LRSC) to the 15 measured ROI time activity curves (Zhou et al., 2003; Zhou et al., 2007). The mean cortical DVR (cDVR) was calculated by averaging the mean DVR values from the orbitofrontal, prefrontal, superior frontal, parietal, lateral temporal, occipital, and anterior and posterior cingulate regions (Villemagne et al., 2008). The cerebellar grey matter was used as the reference region. For voxel-wise analysis, parametric images of DVR were generated by spatially normalizing using an R1 template (R1 = K1/K1 [reference tissue], the target to reference tissue ratio of tracer transport rate constant from vascular space to tissue) (Zhou et al., 2007).

Pseudo-temporal analysis of cross-sectional data via ranking

For voxel-wise analysis, parametric images of DVR were spatially normalized using SPM2 with an R1 template. As defined above, the cDVR value approximates average amyloid deposition in grey matter throughout the brain. To extract the spatial dynamics of amyloid deposition, participants were ranked based on their individual cDVR score, resulting in an across-group waveform for each voxel such that the x-axis is the participants' cDVR score and the y-axis is the DVR value associated with that voxel across the group. When these waveforms were examined, the general pattern was the relative absence of DVR increase, followed by a linear increase in voxel-wise DVR with respect to cDVR value (Figure 1). The aim of the present study was to determine whether some voxels are relatively spared relative to other voxels, e.g., whether the inflection point at which the DVR value in a given voxel starts increasing occurs at a larger cDVR value compared to other voxels. For a given voxel, the signal intensity for *N* subjects may be expressed as:

$$I_i; i=1,\ldots,N. \quad (1)$$

These signal intensities may be pseudo-temporally organized using a function *r(i)*:

$$i \xrightarrow{r(i)} j, \quad (2)$$

which in this case was increasing cDVR score, forming a pseudo-temporal waveform $S_x(t)$:

$$S_x(t) = [I^{(x)}_{r(1)} \dots I^{(x)}_{r(N)}]. \quad (3)$$

The inflection point may be found from this waveform by finding the point *t* at which the derivative is maximized.

The assumption is that there is a spatial spread of amyloid deposition, and by determining when the amyloid increases, the spatial extent of the amyloid "wavefront" can be extracted. To extract this information, each voxel waveform was fitted using a piece-wise linear fit. Each fit was automatically calculated and included least-squares optimization to reduce the squared 2-norm of the residual between the fitted curve and the original waveform. Due to spline smoothing of the data inherent in the fitting process, individual deviations from the assumption of less amyloid deposition earlier in disease progression have less effect over the general pattern.

For each spatial (voxel) location in the brain, three characteristics in relation to amyloid load were quantified from the ^{11}C-PiB PET signal across the group: an inflection point that estimates how much total amyloid must be present in the brain before the voxel exhibits signs of amyloid accumulation, the initial signal intensity (or average ^{11}C-PiB PET signal before the inflection point), and a measure intended to be related to total amyloid accumulation (measured via integration of the signal change after the onset of amyloid accumulation at that point) (Figure 1b). The initial signal intensity is the magnitude of the ^{11}C-PiB PET signal when presumably no amyloid is present, and its spatial distribution is most likely related to blood flow and tracer delivery. The improvement in statistical power using this approach was quantified using simulated data (Supplementary Methods).

Non-specific white matter signal may introduce noise for voxels located within the white matter. Although it is fairly difficult to account for this, our method assumes that there is little to no amyloid accumulation in white matter and we show only surface maps of inflection points or accumulation. Furthermore, this signal should vary randomly across subjects and would introduce a slight increase in the baseline values, resulting in slightly later inflection values if white matter did accumulate amyloid. However, when performing the piece-wise linear fit, we found little evidence of accumulation in white matter (Supplementary Materials).

Subgroup formation

Since change in immediate verbal recall is among the earliest cognitive changes detected during the preclinical phase of Alzheimer's disease (Grober et al., 2008), we used the immediate free recall score (sum of the five learning trials) from the CVLT (Delis et al., 1987) to form sub-groups of stable and declining individuals. The choice to use CVLT is supported by a number of studies on different subject groups showing correlations between composite (i.e., non-temporal) cognitive scores that are highly related to or include the CVLT (Chetelat et al., 2011; Forsberg et al., 2010; Mormino et al., 2009; Pike et al., 2007; Rentz et al.; Storandt et al., 2009; Villemagne et al., 2008). These sub-groups were defined based on cognitive dynamics, or the slope of performance change over all years of each individual's CVLT scores in the years prior to and concurrent with the initial PiB assessment. CVLT slopes were calculated with mixed-effects linear regression using an

interval model with random intercept and slope (no other covariates were included). The cognitively stable (CS) group was defined by individuals in the highest 20% of the CVLT slopes, while the cognitively declining (CD) group showed a pronounced cognitive decline, with CVLT slopes in the lowest 20%. At the time of the PET scan, in the CD group, one subject was diagnosed with MCI and another subject was determined to be cognitively impaired. Later, in the CS group one subject was diagnosed with probable DAT and another developed MCI, while in the CD group one subject was diagnosed with probable DAT, while the MCI and impaired subjects maintained their status. Group demographics are shown in Table 1.

Since the CD group was significantly older and had a trend of higher cDVR values compared to the CS group, we repeated our analyses using age- and cDVR-balanced groups (N=19). The results were similar to those found using the top and bottom 20% CVLT slope groups, and thus we chose the 20% group definition for consistency with previously published literature. Furthermore, we chose to define groups rather than perform regression since our whole-group analysis indicated highly non-linear amyloid deposition progression and regression analyses rely on the assumption of linearity. There were no significant differences in the percentage of amyloid-positive subjects in each group based on either of two previously published thresholds of 1.2 (Sojkova et al., 2011a) and 1.5 (Jack et al., 2009a).

Permutation testing

To determine the significance of the group differences, a permutation test was performed. Subjects in the top and bottom 20% cognitive groups were randomly assigned to two new groups and analyzed as in the original groups. Due to computational constraints and small group sizes, ROIs were manually delineated and the averaged waveform from voxels within the ROI were analyzed. One full analysis requires approximately 5 hours of computation time, arising mostly from the non-linear optimization needed for each voxel-wise spline fit. Beyond computational constraints, the small group sizes prohibit voxel-based comparisons since the fit is less exact (i.e., there is less data) and corrections for multiple comparisons at the voxel-wise level would result in no significantly different voxels. Although it is possible to dramatically decrease computation time by using a vectorized implementation, this approach is incompatible with the non-linear optimization for the spline fits.

Four areas were defined: left and right sensorimotor areas, and left and right temporal areas. These areas were chosen based on large differences in inflection points between the CD and CS groups. An additional four ROIs were also delineated for comparison to previous studies: the left and right precuneus, and the left and right frontal areas. ROIs were not restricted to grey matter, since the images were not segmented, and thus may include some white matter voxels. The probabilities were corrected for multiple comparisons using the False Discovery Rate (FDR) method (Benjamini and Hochberg, 1995). The permutation test was performed 10,000 times to obtain distributions of group differences in inflection (relative sparing) and signal increase (accumulation).

Results

To investigate amyloid distribution as a function of total amyloid burden – our proxy to amyloid deposition dynamics – we analyzed voxel-wise ^{11}C-PiB PET scans from 64 subjects using the aforementioned spline fitting method. By spatially mapping the inflection points and accumulation, patterns of relative sparing of some regions compared to other regions may be observed. In other words, much higher total amyloid burden must be reached before relatively spared regions become affected, and this is reflected in the inflection point maps (called **IPMs** herein).

For better visualization and interpretation of the IPMs, voxels that show relatively late amyloid accumulation (inflection points at higher cDVR values are color-coded in blue, whereas red represents brain regions that are affected early, i.e., at relatively lower cDVR levels. These IPMs are consistent with the histological findings from Braak et al., 1997, in that there is relative sparing of the sensorimotor and occipital cortices at earlier stages of amyloid deposition (Figure 2.I). This pattern is not observed in the initial signal intensities, indicating that it is the signal change due to amyloid deposition that is detected by the inflection points rather than the signal level at the start. Consistent with previous amyloid imaging studies, the precuneus and frontal cortices are affected early, i.e., these regions begin accumulating amyloid when the total amyloid burden for the cortex is relatively low (Figure 2.II).

Spatial Patterns and Cognitive Status

Each subgroup consists of 13 subjects, corresponding to the individuals having the top and bottom 20% CVLT slope scores. As expected, the CVLT slope scores are significantly different. The positive CVLT slope in the CS group reflects a trend of better performance over time due to practice from repeated testing. Age is also significantly different between groups, but total amyloid load expressed as the cDVR score is not significantly different. However, there is a trend of higher cDVR values for the declining group.

Despite the lack of significant differences in mean cortical amyloid load, the spatial patterns of the inflection points between the two groups were found to be divergent in two regions: the temporal lobe and the sensorimotor cortices (Figures 3 and S4). For the CS group, these two regions are relatively spared at early stages, while these regions are impacted earlier (i.e., at lower cDVR levels) in the CD group. In contrast, the patterns for baseline signal intensities and signal increases are not noticeably different between groups, except for greater overall accumulation for the CD group due to the trend of higher cDVR values.

To determine whether the spatial differences in amyloid distribution are significant, we defined four regions of interest (ROIs) in the areas that visually differ: the left and right sensorimotor areas, and the left and right temporal areas (Figure S5). An additional four ROIs were also delineated for comparison to previous studies: the left and right precuneus, and the left and right frontal areas. Permutation of group membership and analysis of the average amyloid signal for voxels within these ROIs for 10,000 permutations resulted in a distribution that could be used to determine significance for the original groups. The results of permutation testing revealed significant differences in inflection and accumulation for the left temporal area, accumulation in the left sensorimotor area, and inflection in the right sensorimotor area (Table 2). Conversely, although there is a trend toward lower accumulation for the frontal areas and right precuneus in the CS group, these trends do not remain significant after correction for multiple comparisons.

Discussion

Spatial Patterns of Amyloid Deposition

We obtained estimates of the spatial progression of amyloid deposition in older adults using ^{11}C-PiB PET imaging and an image analysis method that assumed that the total amyloid burden is a reasonable approximation of the stage of the pathology. This assumption allows the approximation of spatiotemporal patterns from cross-sectional data, leading to estimation of relative sparing of certain brain regions as reflected by relatively later inflection points in regional amyloid signal.

The IPM maps are relative, such that they can only be interpreted in the context of what is occurring elsewhere in the cortex. A lower cDVR inflection point in a particular region

means that this region begins to accumulate amyloid while the rest of the cortex remains relatively free of amyloid.

The spatial patterns are noteworthy in that they synthesize previous findings from both histological and imaging studies. Similar to histological and imaging studies, there is clear sparing of the occipital and sensorimotor areas and evident deposition in the precuneus and frontal regions at early stages of amyloid deposition. Furthermore, there are some noteworthy new findings. Histologically, it was found that subjects exhibited amyloid deposition in a basal-to-apical pattern, but there was no detectable basal-to-apical pattern in the analysis of ^{11}C-PiB PET imaging, a finding similar to other imaging studies. This discrepancy could be due to divergent approaches to quantifying amyloid load. Braak et al. used a silver-pyridine method, which is more selective for nucleation sites (Braak and Braak, 1997a). ^{11}C-PiB labels fibrillar Aβ, i.e., plaques that contain Aβ sheets, and also labels cerebrovascular amyloid angiopathy.

Cognitive Status is related to the Pattern of Amyloid Deposition

Visually, there are large differences in the pattern of amyloid deposition based on cognitive performance, with CD subjects displaying involvement of most of the brain at relatively early stages (low cDVR levels), whereas CS subjects showed relative sparing of the sensorimotor and temporal cortex at low cDVR levels. Also, as the subgroups were defined (top/bottom 20%), the trend of higher DVR values in the declining group plus higher maximum DVR resulted in generally higher accumulation values. Despite the trend of higher DVR, though, direct group comparisons lack the statistical power to detect significant differences. Furthermore, comparison of two groups with matched DVR values achieved similar results for inflection points and accumulation.

Atrophy is a potential confound when analyzing PET imaging data (Meltzer et al., 1990). When we examined atrophy maps for the CS and CD groups, there were significant differences in atrophy in the temporal lobes, the precuneus, and the medial frontal areas, with the CD group having consistently less grey matter than the CS group (Figure S6). Although it is known that there is atrophy, the effect of atrophy on the amyloid deposition analysis is not straightforward. Theoretically, less tissue density would imply less amyloid accumulation and lower PiB-PET signal intensity, such that the entire across-group cDVR curve would shift downwards. If atrophy became more pronounced in conjunction with higher amyloid burden, the rate of amyloid accumulation may also decrease. Since the declining group has significantly more atrophy, the effect would be *less* difference between the stable and declining groups in regions containing atrophy (Figure S7). Furthermore, the pattern of atrophy does not perfectly coincide with the regions that had significantly different amyloid deposition patterns, indicating that it is not the driving force behind the differences between the cognitively stable and declining groups.

In the original Braak & Braak study (Braak and Braak, 1991), it was noted that there was large inter-subject variability in the amyloid patterns, even for subjects with similar total amyloid burden, resulting in definition of only three stages of amyloid deposition progression. This large variability may be due to different spatiotemporal patterns of amyloid deposition, which may in turn be related to differences in cognitive performance, as association cortex may be affected earlier or later depending upon the individual's amyloid deposition trajectory. More importantly, these results suggest that the spatial pattern of amyloid deposition might be a powerful early biomarker of cognitive decline. The current study introduces such a biomarker based on the IPMs and related measures.

A popular model of the developmental course of DAT suggests that one of the earliest detectable changes is increased amyloid load (Jack et al., 2010). Thus the viability of using

CSF Aβ42 or ^{11}C-PiB PET imaging as biomarkers for the early detection of Alzheimer's disease has been investigated (Nordberg et al., 2010; Resnick and Sojkova, 2011). However, differences in amyloid deposition may be subtle, especially for individuals who are cognitively declining but remain clinically nondemented. In our sample, a direct comparison of mean amyloid signal between groups showed a non-significant trend within the ROIs, demonstrating that our IPM-based analysis approach is a more distinctive biomarker of amyloid progression.

Our results indicate that one difficulty of using amyloid as a cross-sectional biomarker for DAT may stem from the fact that it is the spatial pattern that is related to cognitive performance (and perhaps disease progression) rather than the actual amount of amyloid present in the brain at a given time. However, the extent to which amyloid deposition or another neurodegenerative process, e.g., tangle formation, actually triggers cognitive decline remains unclear (Hardy, 2009). Several processes may occur simultaneously and multiple biomarkers may be most informative in predicting cognitive decline. For example, a cross-modality study of regional cerebral blood flow (rCBF) and ^{11}C-PiB load showed divergent patterns of rCBF changes between high- and low-PiB groups, but the pattern included both increases and decreases in rCBF, which is unlikely to be driven solely by amyloid deposition (Sojkova et al., 2008; Vlassenko et al., 2010). More recently, high risk for subsequent cognitive impairment has been shown in cognitively normal individuals with DAT-like cortical thinning and low CSF Aβ (Dickerson and Wolk, 2012).

Furthermore, only one of the subjects in this study was diagnosed with DAT (but not included in the cognitive subgroup analysis), which raises the question whether subjects with DAT have their own unique spatial patterns of amyloid deposition. There is some evidence for this, since studies of these populations have indicated that high ^{11}C-PiB PET signal is most relevant in the bilateral frontal and cingulate cortices in discriminating DAT from healthy subjects, a finding that was not found in our subject pool (Forsberg et al., 2008; Grimmer et al., 2009; Klunk et al., 2004; Price et al., 2005; Rowe et al., 2007). Amyloid load may asymptote at a maximum or plateau, but for the data analyzed in this study, there was no clear upper asymptote, indicating that the complete amyloid load trajectory has not been fully analyzed (Engler et al., 2006; Jack et al., 2009b; Kadir et al., 2010). Furthermore, our method may not be applicable to subject pools that consisted of only amyloid-positive individuals. In this case, there may be an insufficient number of low DVR values, so all regions may be fully saturated with amyloid and appear as an unchanging signal intensity.

Despite the exclusion of DAT subjects in the cognitive subgroup analysis, significant differences were still found within our subject pool when they were grouped based on cognitive performance. Since a large difference was found in a limited sample consisting only of non-DAT subjects, it highlights the potential influence of the spatial pattern of amyloid deposition on cognitive performance in a preclinical disease state. Extension of the analysis approach used in this study to more individuals with mild cognitive impairment might shed light on its relevance for early detection of DAT.

Supplementary Material

Refer to Web version on PubMed Central for supplementary material.

Acknowledgments

This research was supported in part by NIH grant NIA-R01-14971, by the Intramural Research Program of the NIH, National Institute on Aging and by NIA Research and Development Contract HHSN-260-2004-00012C. R. A. Yotter received support from an NIH T-32 Training Grant. We thank the staff of the Johns Hopkins PET facility for their efforts and the BLSA participants for their participation.

References

Benjamini Y, Hochberg Y. Controlling the false discovery rate: a practical and powerful approach to multiple testing. Journal of the Royal Statistical Society Series B (Methodological). 1995; 57:289–300.

Blessed G, Tomlinson BE, Roth M. The association between quantitative measures of dementia and of senile change in the cerebral grey matter of elderly subjects. British Journal of Psychiatry. 1968; 114:797–811. [PubMed: 5662937]

Braak H, Braak E. Neuropathological stageing of Alzheimer-related changes. Acta Neuropathologica. 1991; 82:239–259. [PubMed: 1759558]

Braak H, Braak E. Frequency of stages of Alzheimer-related lesions in different age categories. Neurobiology of Aging. 1997a; 18:351–357. [PubMed: 9330961]

Braak H, Braak E. Staging of Alzheimer-related cortical destruction. International Psychogeriatrics. 1997b; 9:257–261. [PubMed: 9447446]

Chetelat G, Villemagne VL, Pike KE, Ellis KA, Bourgeat P, Jones G, et al. Independent contribution of temporal beta-amyloid deposition to memory decline in the pre-dementia phase of Alzheimer's disease. Brain. 2011; 134:798–807. [PubMed: 21310725]

Clark VH, Resnick SM, Doshi J, Beason-Held LL, Zhou Y, Ferrucci L, et al. Longitudinal imaging pattern analysis (SPARE-CD index) detects early structural and functional changes prior to cognitive decline in healthy older adults. Neurobiology of Aging. in press.

Delis, DC.; Kramer, JH.; Kaplan, E.; Ober, BA. California Verbal Learning Test - Research Edition. New York: The Psychological Corporation; 1987.

Dickerson BC, Wolk DA. MRI cortical thickness biomarker predicts AD-like CSF and cognitive decline in normal adults. Neurology. 2012; 78:84–90. [PubMed: 22189451]

Engler H, Forsberg A, Almkvist O, Blomquist G, Larsson E, Savitcheva I, et al. Two-year follow-up of amyloid deposition in patients with Alzheimer's disease. Brain. 2006; 129:2856–2866. [PubMed: 16854944]

Forsberg A, Almkvist O, Engler H, Wall A, Langstrom B, Nordberg A. High PIB retention in Alzheimers disease is an early event with complex relationship with CSF biomarkers and functional parameters. Current Alzheimer Research. 2010; 7:56–66. [PubMed: 20205671]

Forsberg A, Engler H, Almkvist O, Blomquist G, Hagman Gr, Wall A, et al. PET imaging of amyloid deposition in patients with mild cognitive impairment. Neurobiology of Aging. 2008; 29:1456–1465. [PubMed: 17499392]

Grimmer T, Henriksen G, Wester H Jr, Förstl H, Klunk WE, Mathis CA, et al. Clinical severity of Alzheimer's disease is associated with PIB uptake in PET. Neurobiology of Aging. 2009; 30:1902–1909. [PubMed: 18346821]

Grober E, Hall CB, Lipton RB, Zonderman AB, Resnick SM, Kawas C. Memory impairment, executive dysfunction, and intellectual decline in preclinical Alzheimer's disease. Journal of the International Neuropsychological Society. 2008; 14:266–278. [PubMed: 18282324]

Hardy J. The amyloid hypothesis for Alzheimer's disease: a critical reappraisal. Journal of Neurochemistry. 2009; 110:1129–1134. [PubMed: 19457065]

Jack CR, Knopman DS, Jagust WJ, Shaw LM, Aisen PS, Weiner MW, et al. Hypothetical model of dynamic biomarkers of the Alzheimer's pathological cascade. The Lancet Neurology. 2010; 9:119–128.

Jack CR, Lowe VJ, Senjem ML, Weigand SD, Kemp BJ, Shiung MM, et al. 11C PiB and structural MRI provide complementary information in imaging of Alzheimer's disease and amnestic mild cognitive impairment. Brain. 2008; 131:665–680. [PubMed: 18263627]

Jack CR, Lowe VJ, Weigand SD, Wiste HJ, Senjem ML, Knopman DS, et al. Serial PIB and MRI in normal, mild cognitive impairment and Alzheimer's disease: implications for sequence of pathological events in Alzheimer's disease. Brain. 2009a; 132:1355–1365. [PubMed: 19339253]

Jack CR, Lowe VJ, Weigand SD, Wiste HJ, Senjem ML, Knopman DS, et al. Serial PIB and MRI in normal, mild cognitive impairment and Alzheimer's disease: implications for sequence of pathological events in Alzheimer's disease. Brain. 2009b; 132:1355–1365. [PubMed: 19339253]

Kadir A, Almkvist O, Forsberg A, Wall A, Engler H, Langström B, et al. Dynamic changes in PET amyloid and FDG imaging at different stages of Alzheimer's disease. Neurobiology of Aging. 2010; 33:198.e1–198.e14. [PubMed: 20688420]

Klunk WE, Engler H, Nordberg A, Wang Y, Blomqvist G, Holt DP, et al. Imaging brain amyloid in Alzheimer's disease with Pittsburgh Compound-B. Annals of Neurology. 2004; 55:306–319. [PubMed: 14991808]

Lockhart A, Lamb JR, Osredkar T, Sue LI, Joyce JN, Ye L, et al. PIB is a non-specific imaging marker of amyloid-beta (Aβ) peptide-related cerebral amyloidosis. Brain. 2007; 130:2607–2615. [PubMed: 17698496]

Lopresti BJ, Klunk WE, Mathis CA, Hoge JA, Ziolko SK, Lu X, et al. Simplified quantification of Pittsburgh compound B amyloid imaging PET studies: a comparative analysis. Journal of Nuclear Medicine. 2005; 46:1959–1972. [PubMed: 16330558]

Meltzer CC, Leal JP, Mayberg HS, Wagner HN Jr, Frost JJ. Correction of PET data for partial volume effects in human cerebral cortex by MR imaging. Journal of computer assisted tomography. 1990; 14:561–570. [PubMed: 2370355]

Mintun MA, LaRossa GN, Sheline YI, Dence CS, Lee SY, Mach RH, et al. [11C]PIB in a nondemented population. Neurology. 2006; 67:446–452. [PubMed: 16894106]

Mormino EC, Kluth JT, Madison CM, Rabinovici GD, Baker SL, Miller BL, et al. Episodic memory loss is related to hippocampal-mediated β-amyloid deposition in elderly subjects. Brain. 2009; 132:1310–1323. [PubMed: 19042931]

Morris JC. Clinical Dementia Rating: A reliable and valid diagnostic and staging measure for dementia of the Alzheimer type. International Psychogeriatrics. 1997; 9:173–176. [PubMed: 9447441]

Nordberg A, Rinne JO, Kadir A, Langstrom B. The use of PET in Alzheimer disease. Nat Rev Neurol. 2010; 6:78–87. [PubMed: 20139997]

Pike KE, Savage G, Villemagne VL, Ng S, Moss SA, Maruff P, et al. β-amyloid imaging and memory in non-demented individuals: evidence for preclinical Alzheimer's disease. Brain. 2007; 130:2837–2844. [PubMed: 17928318]

Price JC, Klunk WE, Lopresti BJ, Lu X, Hoge JA, Ziolko SK, et al. Kinetic modeling of amyloid binding in humans using PET imaging and Pittsburgh Compound-B. J Cereb Blood Flow Metab. 2005; 25:1528–1547. [PubMed: 15944649]

Rentz DM, Amariglio RE, Becker JA, Frey M, Olson LE, Frishe K, et al. Face-name associative memory performance is related to amyloid burden in normal elderly. Neuropsychologia. 2011; 49:2776–2783. [PubMed: 21689670]

Resnick S, Sojkova J. Amyloid imaging and memory change for prediction of cognitive impairment. Alzheimer's Research & Therapy. 2011; 3:1–9.

Resnick SM, Sojkova J, Zhou Y, An Y, Ye W, Holt DP, et al. Longitudinal cognitive decline is associated with fibrillar amyloid-beta measured by [11C]PiB. Neurology. 2010; 74:807–815. [PubMed: 20147655]

Rowe CC, Ackerman U, Browne W, Mulligan R, Pike KL, O'Keefe G, et al. Imaging of amyloid β in Alzheimer's disease with 18F-BAY94-9172, a novel PET tracer: proof of mechanism. The Lancet Neurology. 2008; 7:129–135.

Rowe CC, Ng S, Ackermann U, Gong SJ, Pike K, Savage G, et al. Imaging β-amyloid burden in aging and dementia. Neurology. 2007; 68:1718–1725. [PubMed: 17502554]

Shoghi-Jadid K, Small GW, Agdeppa ED, Kepe V, Ercoli LM, Siddarth P, et al. Localization of neurofibrillary tangles and beta-amyloid plaques in the brains of living patients with Alzheimer disease. American Journal of Geriatric Psych. 2002:10.

Sojkova J, Beason-Held L, Zhou Y, An Y, Kraut MA, Ye W, et al. Longitudinal cerebral blood flow and amyloid deposition: An emerging pattern? Journal of Nuclear Medicine. 2008; 49:1465–1471. [PubMed: 18703614]

Sojkova J, Driscoll I, Iacono D, Zhou Y, Codispoti K-E, Kraut MA, et al. In vivo fibrillar {beta}-amyloid detected using [11C] PiB positron emission tomography and neuropathologic assessment in older adults. Archives of neurology. 2011a; 68:232. [PubMed: 21320990]

Sojkova J, Zhou Y, An Y, Kraut MA, Ferrucci L, Wong DF, et al. Longitudinal patterns of {beta}-amyloid deposition in nondemented older adults. Arch Neurol. 2011b; 68:644–649. [PubMed: 21555640]

Storandt M, Mintun MA, Head D, Morris JC. Cognitive decline and brain volume loss as signatures of cerebral amyloid-{beta} peptide deposition identified with Pittsburgh compound B: cognitive decline associated with A{beta} deposition. Archives of Neurology. 2009; 66:1476–1481. [PubMed: 20008651]

Villemagne VL, Pike KE, Chételat G, Ellis KA, Mulligan RS, Bourgeat P, et al. Longitudinal assessment of Aβ and cognition in aging and Alzheimer disease. Annals of Neurology. 2011; 69:181–192. [PubMed: 21280088]

Villemagne VL, Pike KE, Darby D, Maruff P, Savage G, Ng S, et al. Aβ deposits in older non-demented individuals with cognitive decline are indicative of preclinical Alzheimer's disease. Neuropsychologia. 2008; 46:1688–1697. [PubMed: 18343463]

Vlassenko AG, Vaishnavi SN, Couture L, Sacco D, Shannon BJ, Mach RH, et al. Spatial correlation between brain aerobic glycolysis and amyloid-β (Aβ) deposition. Proceedings of the National Academy of Sciences. 2010; 107:17763–17767.

Wong DF, Rosenberg PB, Zhou Y, Kumar A, Raymont V, Ravert HT, et al. in vivo imaging of amyloid deposition in Alzheimer disease using the radioligand 18F-AV-45 (Flobetapir F 18). Journal of Nuclear Medicine. 2010; 51:913–920. [PubMed: 20501908]

Zhou Y, Endres CJ, Brašić JR, Huang S-C, Wong DF. Linear regression with spatial constraint to generate parametric images of ligand-receptor dynamic PET studies with a simplified reference tissue model. Neuro Image. 2003; 18:975–989. [PubMed: 12725772]

Zhou Y, Resnick SM, Ye W, Fan H, Holt DP, Klunk WE, et al. Using a reference tissue model with spatial constraint to quantify [11C]Pittsburgh compound B PET for early diagnosis of Alzheimer's disease. Neuro Image. 2007; 36:298–312. [PubMed: 17449282]

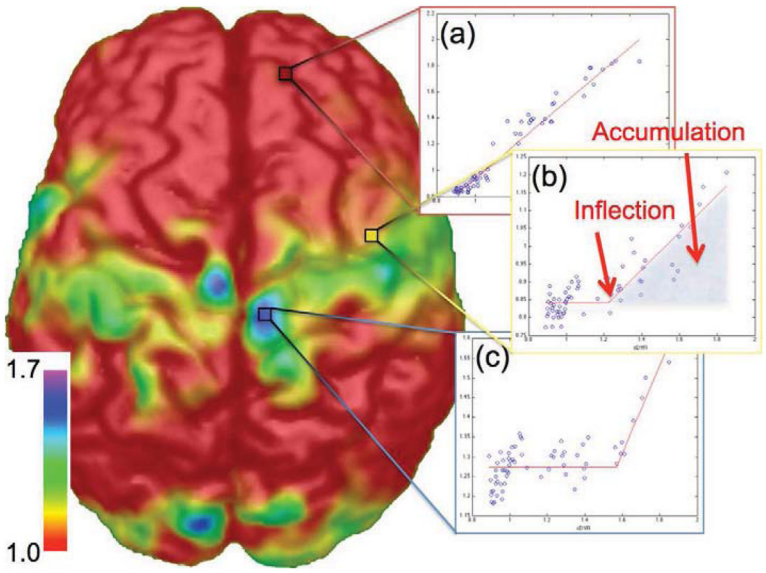

Figure 1. The inflection point is related to the approximate total amyloid load (cDVR) that a subject must reach before amyloid begins accumulating within a region

Shown are three waveforms extracted from a spatial map of inflection points: (a) a voxel that is affected early in the disease progression, (c) a voxel that is affected late in the disease progression, and (b) a voxel between the two extremes. The fitted piecewise linear curve provides information about the initial signal intensity before the inflection point, the total amyloid burden (cDVR) at which the amyloid begins increasing (inflection), and the integral of the curve after the inflection point (accumulation). Colorbar units are cDVR values at which a voxel begins accumulating amyloid. For plots, the x-axis is the cDVR and the y-axis is ^{11}C-PIB signal strength (arbitrary units).

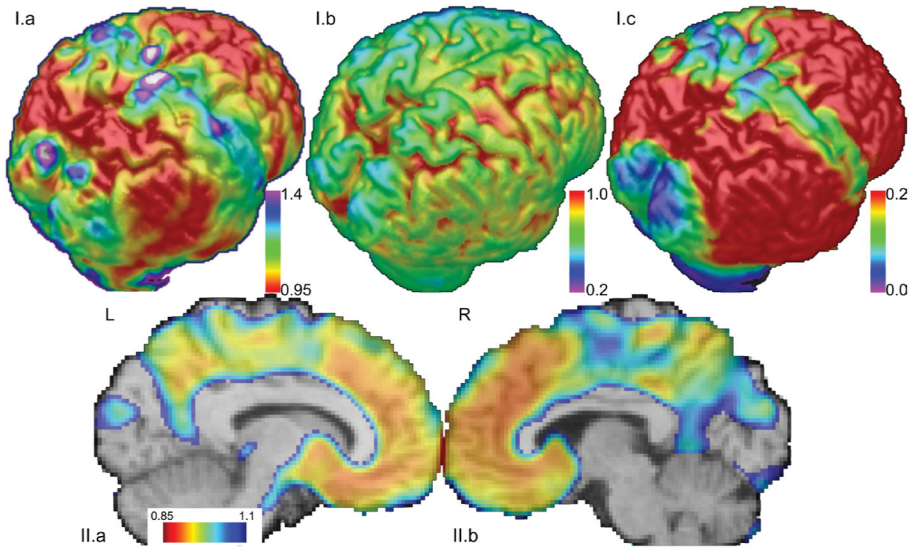

Figure 2. Shown are surface maps of estimated inflection point, initial signal intensity, and accumulation

(I.a) The inflection point at which the voxel-wise PiB signal begins increasing estimates the pattern of progression of amyloid deposition. Higher cDVR needs to be reached before blue/green regions are affected. The occipital and sensorimotor cortices are relatively spared. Units are in total amyloid burden (cDVR) at which the signal begins increasing at a particular voxel. **(I.b) The initial signal intensity has no apparent pattern of sparing.** This suggests that the spatial patterns for the IPM and accumulation maps are due to amyloid signal increase. **(I.c) The amount of amyloid accumulation may be reflected via integration of the curve after the inflection point.** Relatively spared areas are similar to those found via spatial analysis of the inflection point, i.e., the sensorimotor and occipital cortices. Units are signal intensity increase multiplied by cDVR. **(II) Both the precuneus and frontal regions are affected early, i.e., for low cDVR values.** A map of inflection points along the sagittal midline shows that the precuneus and frontal regions begin accumulating amyloid when the total amyloid burden is relatively low.

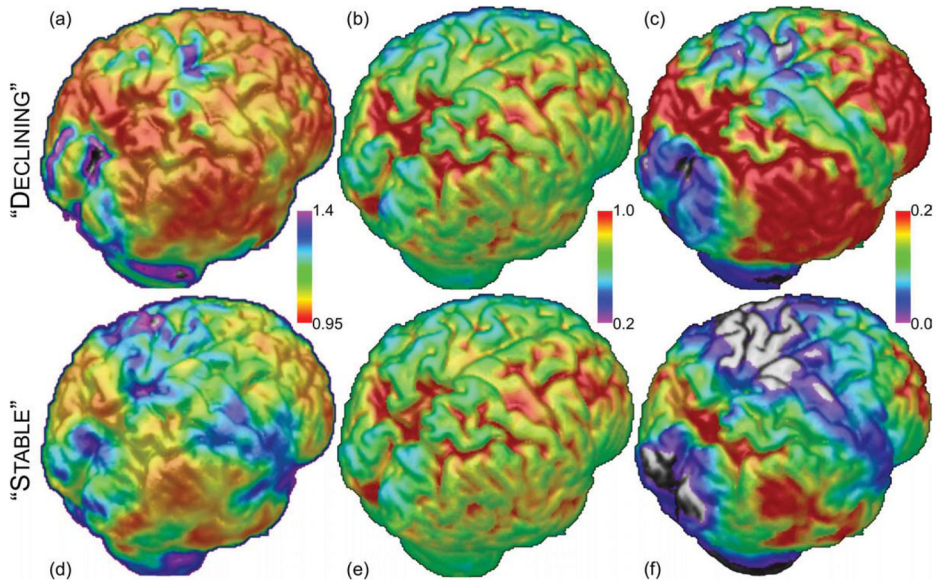

Figure 3. Cognitive status and relative sparing of cortical areas with respect to amyloid load may be related

Shown are surface maps of the IPMs, initial signal intensity, and amyloid accumulation (area under the curve). **(a,d) Relative sparing in the IPM --** in the CS group, the sensorimotor and temporal cortices, plus some other smaller regions, are relatively spared. In the CD group, these regions show signs of amyloid accumulation at relatively low total amyloid burden. The spatial patterns for the IPMs are different. Units for each voxel are cDVR at which the signal at that voxel begins increasing. **(b,e) Initial signal intensity** – Based on visual inspection, the initial signal intensity appear to be similar for both groups. Units are average voxel-wise signal intensity. **(c,f) Accumulation** – Since there is a trend of higher cDVR values for the CD group, there is more accumulation for this group than for the CS group. However, the ratios of values between voxels are highly similar for both groups, meaning that the spatial patterns are highly similar, with the largest difference being a constant offset. Units are signal intensity increase multiplied by cDVR. The implication is that although the spatial distribution of amyloid accumulation is not very different between these groups, the IPMs (a,d) indicate that the spatial pattern of estimated inflection points in amyloid accumulation is the most important discriminant.

Table 1

Group demographics, CVLT, cDVR, and number of amyloid-positive subjects (mean ± standard deviation [range])

	Cognitively Stable (CS) (N=13)	Cognitively Declining (CD) (N=13)	p-value
Age	75.70 ± 5.38 [67.06 – 90.96]	80.70 ± 4.81 [73.47 – 89.48]	0.020
Sex	8 females, 5 males	4 females, 9 males	0.130*
Education (years)	17.15 ± 2.41 (12 – 20)	16.08 ± 2.53 (12 – 19)	0.139
APOE ε4	4 positive	5 positive	0.709*
MMSE	28.92 ± 0.79 (27 – 30)	27.50 ± 2.78 (23 – 30)	0.057
CVLT Slope	1.072 ± 0.403 [0.59 – 2.07]	−0.771 ± 0.654 [−2.81 – −0.25]	1.741e-09
cDVR	1.138 ± 0.206 [0.92 – 1.60]	1.267 ± 0.292 [0.91 – 1.72]	0.207
cDVR > 1.2	5 positive	7 positive	0.458
cDVR > 1.5	1 positive	3 positive	0.305

*Wilcoxon ranked-sum test

Table 2

P-values from permutation testing

ROI	Inflection	Accumulation
Left Temporal Area	0.029*	0.009*
Right Temporal Area	0.097	0.077
Left Sensorimotor Area	0.106	0.015*
Right Sensorimotor Area	0.020*	0.100
Left Frontal Area	0.293	0.036
Right Frontal Area	0.219	0.045
Left Precuneus	0.268	0.105
Right Precuneus	0.056	0.078

Subject groups were permuted to calculate significance of ROI differences between CS and CD groups in inflection (relative sparing) and signal change (accumulation).

*Significant after correction for multiple comparisons using FDR ($p < 0.05$).